





Computation of Armor Losses in AC Submarine Cables

Luca Giussani , Luca Di Rienzo , *Senior Member, IEEE*, Massimo Bechis , and Carlo de Falco 

Abstract—We propose an innovative fast 3D approach for the accurate computation of electromagnetic losses in the metallic armors of submarine cables. In order to develop a scheme that is more efficient with respect to most commonly used 3D simulation methods, typically based on the Finite Element Method (FEM), we proceed by proposing a suitable discretization of an integral formulation. In the proposed approach, each wire of the armor is modeled as filamentary which leads to a dramatic reduction in the number of degrees of freedom in the numerical model and in the overall computational burden. The new approach can be applied to cables where armor wires are stranded either with opposite (con-lay) or same (equilay) orientation as the central phase cables. The efficiency of the proposed method is especially notable in latter case for which FEM is very demanding due to the extremely large model size. The reduction in both computation times and memory footprint allow performing extensive sensitivity studies with respect to geometrical parameters and material properties that would be otherwise unaffordable with existing 3D methods.

Index Terms—Submarine cables, method of moments, eddy currents, magnetic losses.

I. INTRODUCTION

SINCE the installation of the first offshore wind farm on the Denmark coast in 1991 [1], there has been an exponential increase in installed offshore wind capacity, and there is a general agreement that this trend is going to continue in the next few years [2], [3].

An important component of every offshore wind farm is represented by the submarine power cables used to interconnect the different generators of an eolic wind farm and to export the generated power to the mainland.

The proper design of these power cables must take into account several different and often contrasting requirements and constraints. In this respect the thermal behavior of the cables is an important aspect for the overall efficiency and reliability

Manuscript received June 3, 2020; revised September 3, 2020; accepted October 13, 2020. Paper no. TPWRD-00821-2020. (*Corresponding author: Luca Giussani.*)

Luca Giussani and Luca Di Rienzo are with the Dipartimento di Elettronica, Informazione e Bioingegneria, Politecnico di Milano, 20133 Milano, Italy (e-mail: luca.giussani@polimi.it; luca.dirienzo@polimi.it).

Massimo Bechis is with the Prysmian S.p.A., 20126 Milano, Italy (e-mail: massimo.bechis@prysmiangroup.com).

Carlo de Falco is with the MOX - Modeling and Scientific Computing, Dipartimento di Matematica, Politecnico di Milano, 20133 Milano, Italy (e-mail: carlo.defalco@polimi.it).

Color versions of one or more of the figures in this article are available online at <https://ieeexplore.ieee.org>.



Fig. 1. Three-core AC submarine cable.

of the installation: the cables must dissipate the heat generated during their operation in a sufficiently efficient way to avoid overheating phenomena, which can deteriorate the cable itself, and in particular the insulating materials therein.

In order to produce a cable with a satisfactory thermal behavior without recurring to an oversized design, it is crucial to accurately estimate the power losses which occur in the cable.

Fig. 1 shows the structure of a typical submarine AC three-core power cable. The sources of losses are the three-phase conductors, the three conductor sheaths (which protect the enclosed conductors and insulators from seawater), and the external armor (which provides mechanical protection and tensional stability during both the installation and operation of the cable).

The focus of the present article is on the computation of armor losses. For this reason phase conductors are considered filamentary and the presence of sheaths is neglected. These simplifying assumptions lead to an overestimation of armor losses, because both the proximity effect of finite-size conductors and the screening effect of metallic sheaths contribute to a reduction of the magnetic field on the armor.

However we want to emphasize that the formulation presented in this article does not necessarily require these assumptions. Including the sheaths in the model would actually be quite straightforward, by coupling the formulation presented here to the classical integral equation formulation for thin conductive foils presented for example in [4]. As a matter of fact, this will be the subject of a future work [5]. A more refined modelization

of the conductors, on the other hand, would be quite difficult, not for inherent limitations of the presented formulation, but because real world cables do not employ solid-core conductors, which could be easily modeled, but rather Milliken conductors, whose modelization is still an open problem [6], [7].

Most of the existing methods for computation of losses in the armor rely on a 2D description of the cable geometry, with various expedients to include effects caused by the 3D structure of the cable. Fully 3D simulations have been carried out in the recent years, and they provide a high accuracy, but at the price of high computational burden in terms of memory and computational time.

In this paper we present a numerical method for the 3D computation of armor losses which is both accurate and computationally inexpensive. The method extends the integral formulation presented in [8] by deriving formulas for the computation of losses.

In the following, we begin by providing context for this study discussing the existing calculation methods (in Section II) and then pointing out their shortcomings (in Section III); then, in Section IV and Section V we review the discretized integral formulation of [8] while in Section VI we extend it by describing how its solution can be post-processed to obtain estimates of magnetic and electric losses. In Section VII we proceed to compare results of the new method with those of Finite Element Method (FEM) simulations performed with a commercial tool in order to, on the one hand, validate the accuracy of the predictions of the new method and, on the other hand, to assess the performance gain it provides. In Section VIII we use simulation results to discuss the complex interplay between geometrical cable design parameters and material properties in determining the losses. The detailed derivation of the formulas for losses computation used in Section VI is postponed to the Appendix which follows the concluding remarks of Section IX.

II. EXISTING CALCULATION METHODS

Losses in cable armor are commonly computed according to IEC 60287 standard [9]. The semi-empirical formulas contained therein are based on the assumption that the armor can be approximated by a closed pipe [10]. Both armor wires and phase cables, however, are usually helically twisted with different lay lengths. One of the effects of this relative twisting is to prevent circulation of net currents along the armor wires when a balanced three-phase system of currents is supplied to the cable. The calculation method of IEC 60287 standard fails to take this effect into account, leading to an overestimation of armor losses.

Several works try to address this problem by including the effect of twisting in otherwise 2D description of the cable [11]–[14]. While these models manage to suppress the circulation of net currents in armor wires, they do not consider the presence of a magnetic field component parallel to the armor wires, leading in turn to an underestimation of armor losses.

Reference [15] acknowledges the importance of the magnetic field component parallel to the armor wires, and [16] proposes an accurate analytic formula for losses computation which takes into account that component of the magnetic field. However that

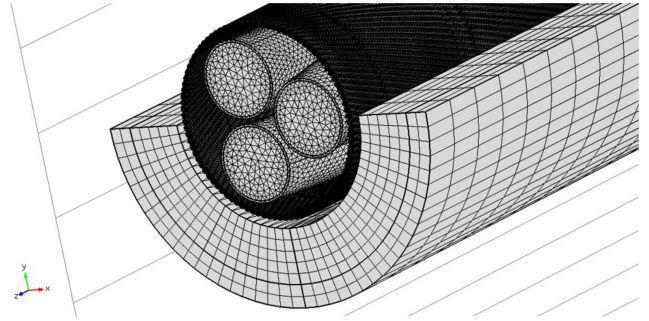


Fig. 2. Example of computational mesh for FEM analysis of submarine cable.

formula is rigorous only when armor wires are straight or sufficiently distant from each other, so that the parallel component of the magnetic field is not influenced by the presence of other wires. When armor wires are twisted this does not hold true. As a matter of fact, the model in [16] is validated against FEM results only for the case of straight and widely spaced wires.

Simplified 2D FEM models and equivalent-circuit models based on an equivalent material representation of the armor are proposed in [17] to take into account the 3D nature of the problem. Unfortunately the accuracy of the proposed models cannot be evaluated since they have not been validated against full 3D FEM models.

A fully 3D modelization of the geometry of a submarine cable therefore could be very useful both for directly computing power losses for real applications and for checking the actual accuracy of simpler models. Only in recent times the advances in computing resources have allowed such an approach. In [18]–[20] 3D FEM simulations of realistic cable geometries are performed. These studies are very valuable for understanding the electromagnetic behavior of submarine cables, but their high computational costs (tens of hours of computing time and tens or hundreds of GB of memory usage for each simulation) make them unsuitable for day to day use in cable design.

III. SHORTCOMINGS OF FINITE ELEMENT ANALYSIS

One of the most widely adopted methods for the 3D computation of losses in submarine cable armor is the FEM. Although this method is potentially very accurate, it is computationally expensive, owing to the high number of degrees of freedom required (see Fig. 2 for a typical computational mesh of a submarine cable).

There are several factors which contribute to the necessity of a high number of elements in the mesh, namely the elongated shape of armor wires, the need to resolve the skin effect caused by the high magnetic permeability of armor wires and the effects of protective layers, such as zinc-galvanizing treatment, the need to discretize also the magnetically inactive regions, and the need to extend the computational domain sufficiently far away from the cable to limit the influence of boundary conditions.

This paper tries to provide a 3D method for the computation of losses in armor wires which addresses the shortcomings of FEM. First of all inside the armor wires an equivalent tensor-valued

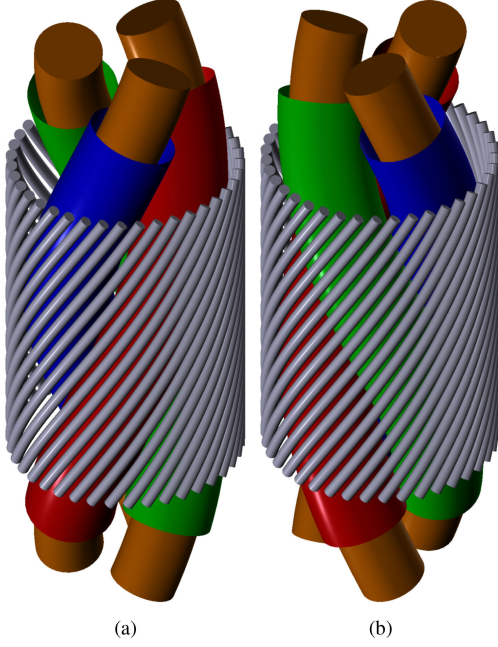


Fig. 3. Structure of submarine AC three-core cable: (a) equilateral configuration (b) contralateral configuration.

permeability is used in place of the actual wire permeability and 162 conductivity. As shown in [8], this allows to take into account 163 the magnetic and eddy currents inside the wires in a simple 164 magnetostatic setting, eliminating the skin effect and relaxing 165 the need to finely mesh the cross section of the wires. Moreover a 166 line integral formulation is adopted. It requires to discretize only 167 the magnetically active regions, leaving the domains occupied by air unmeshed.

Another problem is that the armor of AC submarine cables is usually made of ferromagnetic material (e.g. steel), whose electromagnetic behavior is nonlinear and affected by hysteresis. To rigorously take this aspect into account a nonlinear, time-domain FEM simulation would be required, which would further aggravate the computational cost of the analysis.

A common approach employed to overcome this issue is to approximate the hysteresis behavior of the material by means of a complex valued permeability $\mu_r \in \mathbb{C}$ [21]. By doing so, a single, linear, time-harmonic FEM simulation is enough to analyse the behavior of the cable. In [22] an accurate estimation of complex valued magnetic permeability of a cable armor steel in the presence of a strong skin-effect is carried out. The nonlinear relationship between the magnetic field intensity and the magnetic flux density is linearized since being the magnetic steel armor far from saturated in a typical working condition. The hysteretic behavior is approximated by using a complex valued permeability. This same approach is adopted in this article for both the FEM simulations and the proposed formulation.

IV. MATHEMATICAL MODEL

In [8] it is shown that a thin conductive and magnetic wire can be replaced by a purely magnetic wire characterized by an

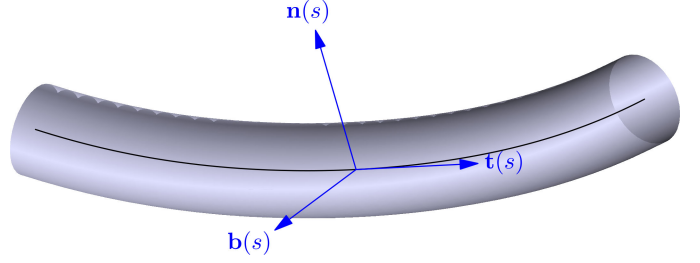


Fig. 4. Local frame of reference along wire.

anisotropic permeability. In other words the constitutive laws of the material

$$\mathbf{B} = \mu_0 \mu_r \mathbf{H} \quad (1)$$

$$\mathbf{J} = \sigma \mathbf{E} \quad (2)$$

are substituted with the following laws

$$\mathbf{B} = \mu_0 K \mathbf{H} \quad (3)$$

$$\mathbf{J} = 0 \quad (4)$$

where K is the permeability tensor, defined in such a way as to take two different values μ_r^{\parallel} and μ_r^{\perp} in the wire axial and transverse directions, to take into account the different behavior of the eddy currents flowing in these two directions.

More precisely, let $\Gamma(s) : [0, L] \rightarrow \mathbb{R}^3$ be the centerline of the wire, parametrized by the curvilinear coordinate s . To every point $\Gamma(s)$ of the centerline we associate a triplet of mutually orthogonal unit vectors $(\mathbf{t}(s), \mathbf{n}(s), \mathbf{b}(s))$, where $\mathbf{t}(s)$ is tangent to Γ , whilst $\mathbf{n}(s)$ and $\mathbf{b}(s)$ are orthogonal both to Γ and to each other (Fig. 4). The tensor permeability along the wire can then be expressed in Cartesian coordinates as

$$K(s) = Q(s) M Q^T(s) \quad (5)$$

where

$$M = \begin{bmatrix} \mu_r^{\parallel} & 0 & 0 \\ 0 & \mu_r^{\perp} & 0 \\ 0 & 0 & \mu_r^{\perp} \end{bmatrix} \quad (6)$$

and

$$Q(s) = \begin{bmatrix} t_x(s) & n_x(s) & b_x(s) \\ t_y(s) & n_y(s) & b_y(s) \\ t_z(s) & n_z(s) & b_z(s) \end{bmatrix} \quad (7)$$

The two values μ_r^{\parallel} and μ_r^{\perp} depend on the wire geometrical and physical parameters (radius r , conductivity σ , permeability μ_r) and on the angular frequency $\omega = 2\pi f$ of the external magnetic 209 field. They are given by [8], [17]

$$\mu_r^{\parallel} = \mu_r \frac{2 J_1(kr)}{kr J_0(kr)} \quad (8)$$

$$\mu_r^{\perp} = \mu_r \frac{J_1(kr)}{kr J_1'(kr)} \quad (9)$$

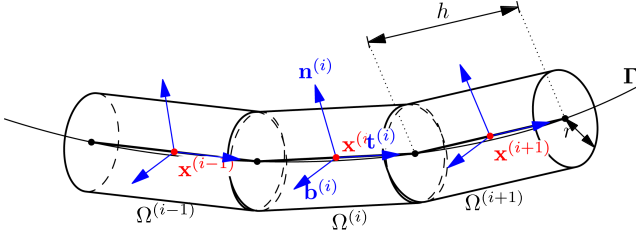


Fig. 5. Wire geometry discretization.

where

$$k = j\sqrt{j\omega\sigma\mu_0\mu_r} \quad (10)$$

and J_α is the order- α Bessel function of the first kind.

Using the equivalent permeability (8) and (9) allows to model the effect of both magnetization and eddy currents up to the dipole moment. Higher order moments are not considered. When armor wires are very close to each other this can introduce inaccuracies.

The three-phase conductors are modeled as infinitely long helical filamentary conductors, each one carrying a known current. Under this assumption the magnetic field generated by the phase conductors at any point of the space can be computed by means of analytical formulas [23].

V. NUMERICAL DISCRETIZATION SCHEME

We use a formulation with wire magnetization \mathbf{M} as unknown. The relation between the magnetization \mathbf{M} and the fields \mathbf{B} and \mathbf{H} is given by

$$\mathbf{B} = \mu_0(\mathbf{H} + \mathbf{M}) \quad (11)$$

By substituting (11) inside (3), we get the basic equation of our formulation

$$\mathbf{M} = \frac{1}{\mu_0} (I - K^{-1}) \mathbf{B} \quad (12)$$

where I indicates the identity operator. The total magnetic field \mathbf{B} in (12) can be split into two contributions as

$$\mathbf{B} = \mathbf{B}^{ext} + \mathbf{B}^M \quad (13)$$

where the term \mathbf{B}^{ext} denotes the magnetic field generated by the phase conductors, and the term \mathbf{B}^M denotes the magnetic field generated by the wire magnetization itself.

Equation (12) cannot be solved in closed form and must be treated numerically. The geometry of the armor wires is discretized into N cylinders as show in Fig. 5. Then the permeability tensor in each cylinder Ω_i , $i = 1, \dots, N$ is a constant matrix (denoted by K_i). We assume that also the magnetization is constant in each cylinder Ω_i and we denote it by \mathbf{M}_i . The unknowns of the problem are thus the N values of the magnetization \mathbf{M}_i .

In order to find N independent equations for these unknowns we collocate (12) at the centers \mathbf{x}_i of the cylinders

$$\mathbf{M}(\mathbf{x}_i) = \frac{1}{\mu_0} (I - K^{-1}(\mathbf{x}_i)) (\mathbf{B}^{ext}(\mathbf{x}_i) + \mathbf{B}^M(\mathbf{x}_i)) \quad (14)$$

Of course from the previous discussion, $\mathbf{M}(\mathbf{x}_i) = \mathbf{M}_i$, and $K^{-1}(\mathbf{x}_i) = K_i^{-1}$. Concerning $\mathbf{B}^{ext}(\mathbf{x}_i)$, it can be computed by means of analytical formulas [23] (and will be denoted by \mathbf{B}_i^{ext} in the following). The term $\mathbf{B}^M(\mathbf{x}_i)$ instead can be written as

$$\mathbf{B}^M(\mathbf{x}_i) = \sum_{j=1}^N \mathbf{B}_{i,j}^M \quad (15)$$

where $\mathbf{B}_{i,j}^M$ is the magnetic field produced by cylinder Ω_j , magnetized with magnetization \mathbf{M}_j , at the center \mathbf{x}_i of cylinder Ω_i . It can be shown [8] that $\mathbf{B}_{i,j}^M$ can be expressed as the surface integral

$$\mathbf{B}_{i,j}^M = -\frac{\mu_0}{4\pi} \int_{\partial\Omega_j} (\mathbf{n} \times \mathbf{M}_j) \times \frac{\mathbf{x}_i - \mathbf{x}}{|\mathbf{x}_i - \mathbf{x}|^3} d\sigma \quad (16)$$

Then (12) can be written as

$$\mathbf{M}_i = \frac{1}{\mu_0} (I - K_i^{-1}) \left(\mathbf{B}_i^{ext} + \sum_{j=1}^N \mathbf{B}_{i,j}^M \right) \quad (17)$$

A straightforward implementation of (17) leads to a linear system whose matrix is full. The computational cost of assembling the matrix however can be greatly reduced by taking into account the symmetries characterizing the cable geometry, which confer a block-circulant structure to the matrix. This particular structure can be exploited both during the matrix assembly and the linear system solution phases [24].

VI. COMPUTATION OF LOSSES

As already stated in Section II, the overall shape of armor wires and their path along the cable has a noticeable effect on armor losses. For this reason (17) takes into account the detailed path Γ of armor wires through the term $\mathbf{B}_{i,j}^M$, which depends on the physical positions of the wire segments Ω_j , which in turn are determined by the paths of the armor wires.

Once the distribution of magnetization \mathbf{M} along the armor wires is determined, however, the wires detailed geometry can be safely disregarded, and losses computation can be carried out using formulas valid for straight and infinitely long conducting and magnetic cylinders placed in a uniform magnetic field.

This approximation is justified by the fact that in a typical submarine cable, the radius of armor wires is much smaller than both the laying pitch and the cable radius, hence armor wires are locally almost straight. Moreover the variations of magnetic field along the wire are slow enough that the magnetic field can be assumed locally uniform.

Let \mathbf{H}_0 be the value of magnetic field at a given point of the wire axis. \mathbf{H}_0^{\parallel} and \mathbf{H}_0^{\perp} are the components parallel and perpendicular to the axis of the wire respectively.

Then the losses value per unit length of wire at that point is given by

$$P = \frac{2\pi}{\sigma} \left[\frac{\text{Re}[-krJ_0(k^*r)J_1(kr)]}{|J_0(kr)|^2} |\mathbf{H}_0^{\parallel}|^2 + \frac{8\text{Re}[-krJ_1(kr)J_1'(k^*r)]}{|(\mu_r + 1)J_0(kr) + (\mu_r - 1)J_2(kr)|^2} |\mathbf{H}_0^{\perp}|^2 \right] \quad (18)$$

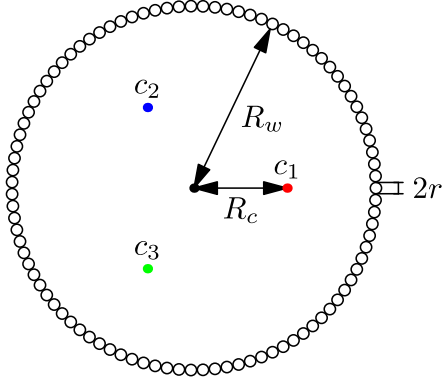
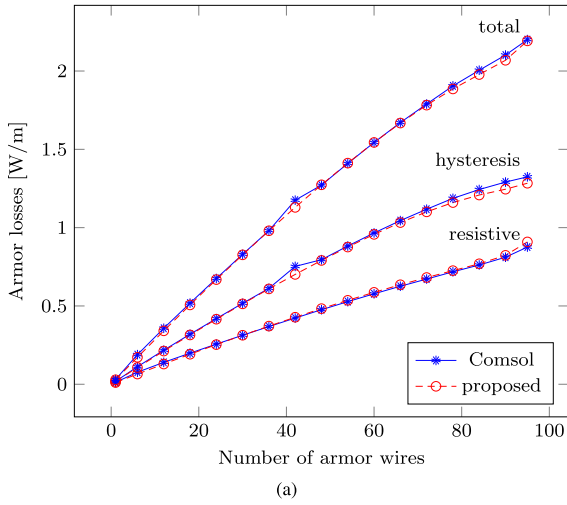
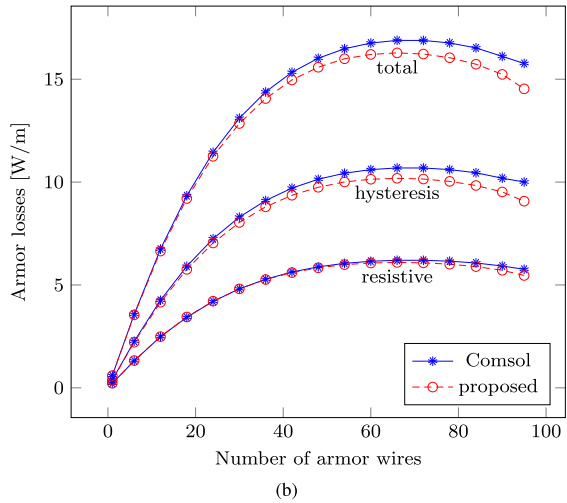


Fig. 6. Cross-section of the cable used for validation.



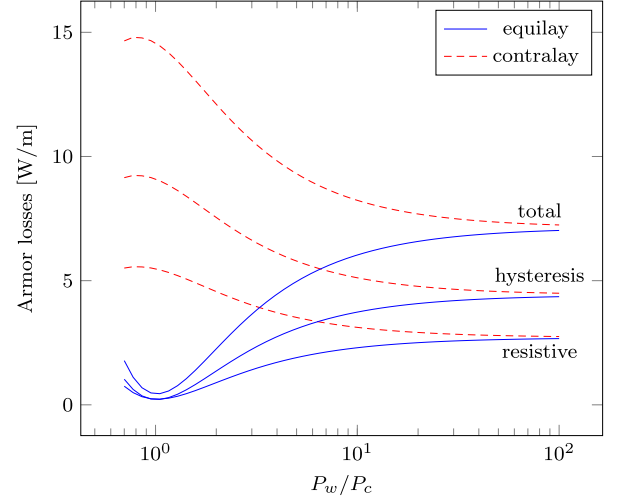
(a)



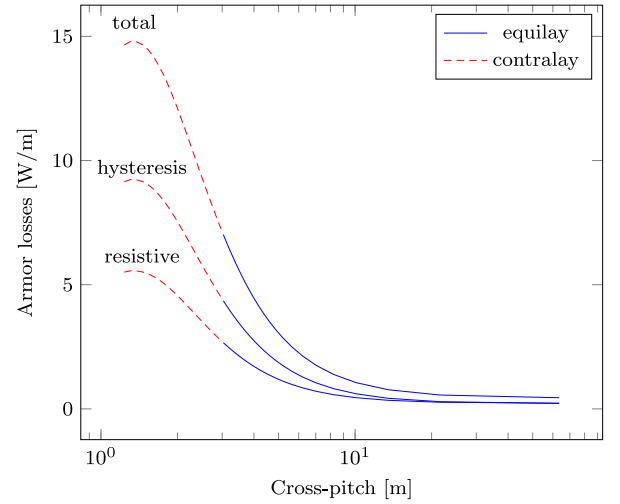
(b)

Fig. 7. Losses per unit length of cable for various number of armor wires: (a) equilay configuration (b) contralay configuration.

A detailed derivation of (18) is included in the Appendix, where the splitting of the total losses P into the resistive component $2\pi P_r$ and hysteresis component P_h can be found as well.



(a)



(b)

Fig. 8. Losses per unit length of cable for different values of armor pitch: (a) as a function of the ratio p_w/p_c (b) as a function of the cross-pitch.

Before using (18), it is necessary to relate the external magnetic field \mathbf{H}_0 to the magnetization \mathbf{M} , which is the unknown of the proposed formulation (17).

Since the proposed approach, as explained in Section IV, reduces the problem to a magnetostatic formulation with a modified tensor permeability, the relation between \mathbf{H}_0 and \mathbf{M} should be found by considering an infinitely long, straight wire, whose tensor permeability is given by (6), placed in a uniform static magnetic field \mathbf{H}_0 .

The solution of the problem can be found in [25]:

$$\mathbf{H}_0^{\parallel} = \frac{1}{\mu_r^{\parallel} - 1} \mathbf{M}^{\parallel} \quad (19)$$

$$\mathbf{H}_0^{\perp} = \frac{1}{2} \frac{\mu_r^{\perp} + 1}{\mu_r^{\perp} - 1} \mathbf{M}^{\perp} \quad (20)$$

where \mathbf{M}^{\parallel} and \mathbf{M}^{\perp} are the parallel and transverse components of \mathbf{M} with respect to the wire.

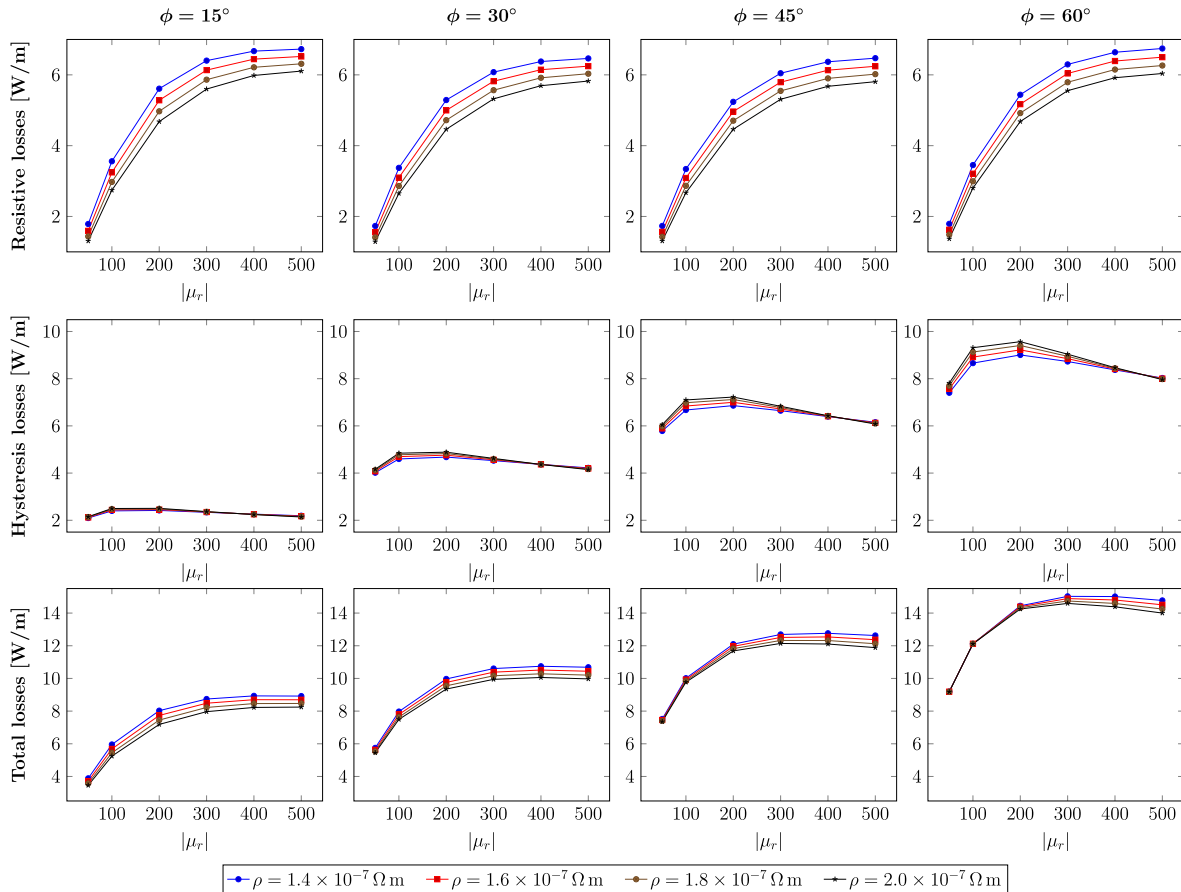


Fig. 9. Sensitivity study of losses per unit length of cable as a function of armor wire resistivity and complex permeability (modulus and angle).

VII. VALIDATION OF THE METHOD

The method is validated by comparing its results with those obtained using the commercial FEM software Comsol, for a cable whose cross-section is shown in Fig. 6. The FEM calculations explicitly model eddy currents in armor wires, without resorting to the equivalent tensor valued permeability model presented before.

The radius of the armor wires is $r = 3.5$ mm. Their distance from the axis of the cable is $R_w = 110$ mm. The distance of the three-phase conductor c_1 , c_2 , and c_3 from the axis of the cable is $R_c = 57$ mm. As already said, the three-phase conductor are modeled as filamentary conductors carrying a system of three-phase currents of known value $I = 800A_{\text{rms}}$. Although it is not apparent from Fig. 6, both the armor wires and the phase conductors are helically twisted (Fig. 3), with twisting pitches $p_w = 2$ m and $p_c = 3$ m respectively. We designate by the term *equilay* a cable in which the twisting directions of the armor wires and the phase conductors are the same. Vice versa, if the twisting directions are opposed, we speak of a *contralay* cable.

For the sake of validation, the complex permeability of the armor wires is fixed at $\mu_r = |\mu_r|e^{-\phi i}$ with $|\mu_r| = 300$ and $\phi = 60^\circ$ and the resistivity is fixed at $\rho = 2.08E-7 \Omega\text{m}$. These values are coherent with measurements performed internally

by Prysmian S.p.A. This choice of physical parameters leads to values $|\mu_r^{\parallel}| = 179.97$, $\phi^{\parallel} = 70.13^\circ$ for the longitudinal permeability and $|\mu_r^{\perp}| = 127.33$, $\phi^{\perp} = 74.42^\circ$ for the transverse permeability. The number of armor wires is varied from 1 to 95, even if the lower values are not used in practice. Resistive and hysteresis losses computed by FEM and by the proposed method are compared in Fig. 7, and a good agreement is obtained. Larger differences are observed in the results of hysteresis losses in the contralay case, which is probably a consequence of ignoring moments higher than dipole in the magnetization and eddy current distribution in the wires.

The simulations using the proposed method have been performed on a standard laptop computer, with the most expensive simulation requiring approximately 90s and 1 GB of memory. On the other hand, FEM simulations demand much larger computational resources and have been carried out on a computing server, with the most expensive simulation requiring approximately 33 h and 1300 GB of memory.

VIII. RESULTS

The dramatic improvement in computational time and memory requirement of the proposed method allows extensive simulation campaigns that would be practically unfeasible using

FEM. Except where explicitly noted, the geometrical and physical parameters used in this section are the same as the ones used for the validation, and the armor is made of 95 wires.

A first analysis is carried out computing losses vs. the ratio of the twisting pitch of the armor wires and the one of the phase conductors (Fig. 8). The phase conductors laying pitch is held fixed at $p_c = 3$ m, while the armor laying pitch p_w is varied between 2.1 m and 300 m both for the equilay and contralay configurations. Some of the combinations of armor and conductors lay-lengths used for constructing Fig. 8 are not used in practice but are included nonetheless in order to give a complete picture of the theoretical behavior of losses with respect to these two parameters. The configurations not used in practice are equilay with $p_w \approx p_c$ (mechanically weak) and $p_w \gg p_c$ (almost straight armor wires).

The minimum losses are attained in the equilay configuration with $p_w \approx p_c$, which is unfortunately a condition of poor mechanical robustness. Furthermore even if equilay configurations are characterized by lower armor losses than contralay configurations, the latter are preferred for deep installations due to mechanical reasons [26].

Fig. 9 shows the behavior of losses as the physical parameters of the steel armor (resistivity ρ , complex permeability modulus $|\mu_r|$, complex permeability angle ϕ) are varied. Resistive losses increase with $|\mu_r|$, while they are insensitive to the angle. On the other hand, hysteresis losses are less sensitive to $|\mu_r|$ and, as expected, much more sensitive to the angle of μ_r . The increase of the total losses with $|\mu_r|$ and with the angle is an important suggestion for the choice of the material.

IX. CONCLUSION

The proposed numerical method is based on an integral approach and on some approximations inspired by the physical insight of the involved eddy current phenomena, described by analytical formulas. It reveals to be much more efficient than any general purpose approach using a FEM commercial software. Dramatically reducing the computational times and the memory requirements, the new method allows extensive low cost simulation campaigns in the design phase of submarine cables. In particular, the effects of the variation of steel properties and of the laying pitch on the armor losses has been investigated.

APPENDIX

We consider an infinitely long, straight wire of radius r , conductivity σ and complex permeability $\mu_r = |\mu_r|e^{-j\phi}$. For convenience we define both a cartesian coordinate system (x, y, z) and a cylindrical coordinate system (ρ, θ, z) whose z -axes both coincide with the axis of the wire. Let $(\mathbf{e}_x, \mathbf{e}_y, \mathbf{e}_z)$ and $(\mathbf{e}_\rho, \mathbf{e}_\theta, \mathbf{e}_z)$ denote the unit vectors associated to the cartesian and cylindrical coordinate systems respectively (Fig. 10).

The wire is subject to a uniform time-harmonic magnetic field \mathbf{H}_0 , which can be decomposed into two components: \mathbf{H}_0^\parallel , parallel to the wire, and \mathbf{H}_0^\perp perpendicular to the wire. Without loss of generality we can write $\mathbf{H}_0^\parallel = H_0^\parallel \mathbf{e}_z$ and $\mathbf{H}_0^\perp = H_0^\perp \mathbf{e}_x$.

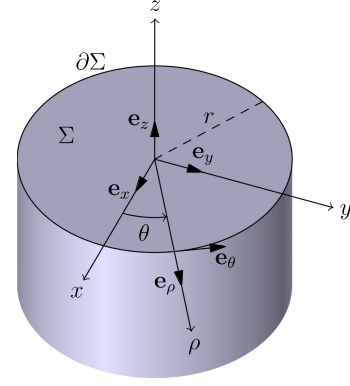


Fig. 10. Reference frame for losses computation.

The external magnetic field generates power losses in the wire, whose total value is the sum of two contributions, namely resistive losses and hysteresis losses. We indicate the time-averaged, per-unit-length value of total, resistive, and hysteresis losses by P , P_r , and P_h respectively.

Total losses can be computed as the real part of the flux of the Poynting vector $\mathbf{S} = \mathbf{E} \times \mathbf{H}^*$ entering the boundary $\partial\Sigma$ of the wire cross section

$$\begin{aligned} P &= \int_{\partial\Sigma} \text{Re} [\mathbf{E} \times \mathbf{H}^*] \cdot (-\mathbf{n}) d\ell \\ &= \int_0^{2\pi} \text{Re} [\mathbf{E}(r, \theta) \times \mathbf{H}^*(r, \theta)] \cdot (-\mathbf{e}_\rho) r d\theta \end{aligned} \quad (21)$$

Computing the resistive and hysteresis contributions requires instead an integration on the wire cross section Σ :

$$\begin{aligned} P_r &= \int_{\Sigma} \text{Re} [\mathbf{J} \cdot \mathbf{E}^*] dA \\ &= \sigma \int_{\Sigma} |\mathbf{E}|^2 dA \\ &= \sigma \int_0^r \int_0^{2\pi} |\mathbf{E}(\rho, \theta)|^2 \rho d\theta d\rho \end{aligned} \quad (22)$$

$$\begin{aligned} P_h &= \int_{\Sigma} \text{Re} [j\omega \mathbf{B} \cdot \mathbf{H}^*] \\ &= \text{Re} [j\omega \mu_0 \mu_r] \int_{\Sigma} |\mathbf{H}|^2 dA \\ &= \text{Re} [j\omega \mu_0 \mu_r] \int_0^r \int_0^{2\pi} |\mathbf{H}(\rho, \theta)|^2 \rho d\theta d\rho \end{aligned} \quad (23)$$

In order to actually compute P , P_r , and P_h , it is therefore necessary to know the distribution of the electric field $\mathbf{E}(\rho, \theta)$ and of the magnetic field $\mathbf{H}(\rho, \theta)$ on the wire cross section. These expressions can be found in [27]. We have that

$$\mathbf{E}^\parallel(\rho, \theta) = H_0^\parallel \frac{k}{\sigma} \frac{J_1(k\rho)}{J_0(kr)} \mathbf{e}_\theta \quad (24)$$

$$\mathbf{H}^\parallel(\rho, \theta) = H_0^\parallel \frac{J_0(k\rho)}{J_0(kr)} \mathbf{e}_z \quad (25)$$

for the fields generated by the axial component \mathbf{H}_0^{\parallel} , and

$$\mathbf{E}^{\perp}(\rho, \theta) = 4H_0^{\perp} \frac{k J_1(k\rho)}{\sigma F(kr)} n\theta \mathbf{e}_z \quad (26)$$

$$\mathbf{H}^{\perp}(\rho, \theta) = 4H_0^{\perp} \left(\frac{J_1(k\rho)}{k\rho F(kr)} \cos\theta \mathbf{e}_{\rho} - \frac{J_1'(k\rho)}{F(kr)} n\theta \mathbf{e}_{\theta} \right) \quad (27)$$

for the fields generated by the transverse component \mathbf{H}_0^{\perp} , where

$$F(kr) = (\mu_r + 1)J_0(kr) + (\mu_r - 1)J_2(kr) \quad (28)$$

Substituting first (24)–(25), and then (26)–(27) inside (21), the total losses due to the axial and transverse components of the magnetic field can be computed

$$P^{\parallel} = \frac{2\pi}{\sigma} \frac{\text{Re}[-krJ_0(k^*r)J_1(kr)]}{|J_0(kr)|^2} |\mathbf{H}_0^{\parallel}|^2 \quad (29)$$

$$P^{\perp} = \frac{16\pi}{\sigma} \frac{\text{Re}[-krJ_1(kr)J_1'(k^*r)]}{|F(kr)|^2} |\mathbf{H}_0^{\perp}|^2 \quad (30)$$

Substituting (24) and (26) inside (22) and performing the integral in θ leads to

$$P_r^{\parallel} = \frac{2\pi}{\sigma} \frac{|k|^2}{|J_0(kr)|^2} |\mathbf{H}_0^{\parallel}|^2 \int_0^r k\rho J_1(k\rho) J_1(k^*\rho) d\rho \quad (31)$$

$$P_r^{\perp} = \frac{16\pi}{\sigma} \frac{|k|^2}{|F(kr)|^2} |\mathbf{H}_0^{\perp}|^2 \int_0^r k\rho J_1(k\rho) J_1(k^*\rho) d\rho \quad (32)$$

The integrals appearing in (31) and (32) are Lommel's integrals, whose general form is [28]

$$\begin{aligned} & (\alpha^2 - \beta^2) \int x J_n(\alpha x) J_n(\beta x) dx \\ &= x [\beta J_{n-1}(\beta x) J_n(\alpha x) - \alpha J_{n-1}(\alpha x) J_n(\beta x)] \quad (33) \end{aligned}$$

Using (33) to evaluate the integrals in (31) and (32) yields the resistive contribution to the losses

$$P_r^{\parallel} = \frac{2\pi}{\sigma} \frac{|k|^2}{|J_0(kr)|^2} \frac{\text{Im}(k^*r J_0(k^*r) J_1(kr))}{\text{Im}(k^2)} |\mathbf{H}_0^{\parallel}|^2 \quad (34)$$

$$P_r^{\perp} = \frac{16\pi}{\sigma} \frac{|k|^2}{|F(kr)|^2} \frac{\text{Im}(k^*r J_0(k^*r) J_1(kr))}{\text{Im}(k^2)} |\mathbf{H}_0^{\perp}|^2 \quad (35)$$

The hysteresis contribution can finally be computed as the difference between the total losses (29) and (30) and the resistive losses (34) and (35).

$$P_h^{\parallel} = P^{\parallel} - P_r^{\parallel} \quad (36)$$

$$P_h^{\perp} = P^{\perp} - P_r^{\perp} \quad (37)$$

REFERENCES

- [1] F. Olsen and K. Dyre, "Vindeby off-shore wind farm-construction and operation," *Wind Eng.*, pp. 120–128, 1993.
- [2] K. Ohlenforst *et al.*, "Global wind report 2018," Global Wind Energy Council, Brussels, Belgium, Tech. Rep., Apr. 2019.
- [3] S. Rodrigues, C. Restrepo, E. Kontos, R. T. Pinto, and P. Bauer, "Trends of offshore wind projects," *Renewable Sustain. Energy Rev.*, vol. 49, pp. 1114–1135, 2015.
- [4] J. Blum, C. Leloup, L. Dupas, and B. Thooris, "Eddy current calculations for the Tore Supra Tokamak," *IEEE Trans. Magn.*, vol. 19, no. 6, pp. 2461–2464, Nov. 1983.
- [5] L. Giussani, L. Di Rienzo, M. Bechis, and C. de Falco, "Fully coupled computation of losses in metallic sheaths and armor of AC submarine cables," *in preparation*.
- [6] R. Benato and A. Paolucci, "Multiconductor cell analysis of skin effect in Milliken type cables," *Electric Power Syst. Res.*, vol. 90, pp. 99–106, Sep. 2012.
- [7] "Large cross-sections and composite screens design," *CIGRE Tech. Brochure*, 2005.
- [8] L. Giussani, M. Bechis, C. de Falco, and L. Di Rienzo, "An integral formulation for an array of wires in a 3-d magneto-quasi-static field," *IEEE Trans. Magn.*, vol. 54, no. 7, pp. 1–8, Jul. 2018.
- [9] International Electrotechnical Commission, "IEC 60287: Electric cables-Calculation of the current rating," 2006.
- [10] J. S. Barrett and G. J. Anders, "Circulating current and hysteresis losses in screens, sheaths and armour of electric power cables – mathematical models and comparison with IEC Standard 287," *IEE Proc. - Sci., Meas. Technol.*, vol. 144, no. 3, pp. 101–110, May 1997.
- [11] J. Bremnes, G. Evensen, and R. Stølan, "Power loss and inductance of steel armoured multi-core cables: Comparison of IEC values with 2.5 D FEA results and measurements," *Proc. CIGRE Session*, 2010.
- [12] N. Viafora, M. Baú, L. M. B. Dall, C. S. Hansen, T. Ebdrup, and F. da Silva, "Analytical expression of equivalent transverse magnetic permeability for three-core wire armoured submarine cables," in *Proc. 51st Int. Universities Power Eng. Conf.*, Sep. 2016.
- [13] M. Baú, N. Viafora, C. S. Hansen, L. M. Bergholdt Dall, T. Ebdrup, and F. Faria da Silva, "Steady state modelling of three-core wire armoured submarine cables: Power losses and ampacity estimation based on FEM and IEC," in *Proc. 51st Int. Universities Power Eng. Conf.*, Sep. 2016, pp. 1–6.
- [14] B. Gustavsen, M. Høyser-Hansen, P. Triverio, and U. R. Patel, "Inclusion of wire twisting effects in cable impedance calculations," *IEEE Trans. Power Del.*, vol. 31, no. 6, pp. 2520–2529, Dec. 2016.
- [15] M. Hatlo and J. Bremnes, "Current dependent armour loss in three-core cables: Comparison of FEA results and measurements," *Proc. CIGRE Session*, 2014.
- [16] M. Hatlo, E. Olsen, R. Stolan, and J. Karlstrand, "Accurate analytic formula for calculation of losses in three-core submarine cables," in *Proc. 9th Int. Conf. Insulated Power Cables*, 2015.
- [17] K. F. Goddard, J. A. Pilgrim, R. Chippendale, and P. L. Lewin, "Induced losses in three-core sl-type high-voltage cables," *IEEE Trans. Power Del.*, vol. 30, no. 3, pp. 1505–1513, Jun. 2014.
- [18] S. Sturm, J. Paulus, K.-L. Abken, and F. Berger, "Estimating the losses in three-core submarine power cables using 2D and 3D FEA simulations," in *Proc. 9th Int. Conf. Insulated Power Cables*, 2015.
- [19] R. Benato and S. Sessa, "A new multiconductor cell three-dimension matrix-based analysis applied to a three-core armoured cable," *IEEE Trans. Power Del.*, vol. 33, no. 4, pp. 1636–1646, Aug. 2018.
- [20] J. C. Del-Pino-López, M. Hatlo, and P. Cruz-Romero, "On Simplified 3D Finite Element Simulations of Three-Core Armoured Power Cables," *Energies*, vol. 11, no. 11, Nov. 2018, Art. no. 3081.
- [21] D. Lederer and A. Kost, "Modelling of nonlinear magnetic material using a complex effective reluctivity," *IEEE Trans. Magn.*, vol. 34, no. 5, pp. 3060–3063, Sep. 1998.
- [22] Y. Ivanenko and S. Nordebo, "Estimation of complex valued permeability of cable armour steel," 2016, pp. 830–833.
- [23] R. Hagel, L. Gong, and R. Unbehauen, "On the magnetic field of an infinitely long helical line current," *IEEE Trans. Magn.*, vol. 30, no. 1, pp. 80–84, Jan. 1994.
- [24] T. De Mazancourt and D. Gerlic, "The inverse of a block-circulant matrix," *IEEE Trans. Antennas Propag.*, vol. 31, no. 5, pp. 808–810, Sep. 1983.
- [25] J. A. Stratton, *Electromagnetic Theory*. New York, NY, USA: McGraw-Hill, 1941.
- [26] T. Worzyk, *Submarine Power Cables: Design, Installation, Repair, Environmental Aspects*. Berlin, Germany: Springer Science & Business Media, 2009.
- [27] J. Lammeraner and M. Štafl, *Eddy Currents*. Boca Raton, FL, USA: CRC Press, 1966, 499.
- [28] F. Bowman, *Introduction to Bessel Functions*. Chelmsford, MA, USA: Courier Corporation, 2012.